Journal of Superconductivity and Novel Magnetism (2025) 38:49
https://doi.org/10.1007/s10948-024-06876-6

RESEARCH

Modelling of Angular Behaviour of Core Loss in Grain-Oriented Laminations Using the Loss Separation Approach

Sai Ram Boggavarapu[1] · Ajay Pal Singh Baghel[2] · Krzysztof Chwastek[3] · Shrikrishna V. Kulkarni[4] · Laurent Daniel[5,6] · Marcos Flavio de Campos[7] · Ikenna Cajetan Nlebedim[2]

Received: 30 December 2023 / Accepted: 23 September 2024

Abstract

An approach to model the anisotropic behaviour of core losses in grain-oriented laminations that are used in advanced electrical machines and transformers is proposed in this work. Core losses are usually split into static hysteresis loss, classical eddy current loss, and excess loss. The static hysteresis and excess loss components exhibit strongly anisotropic behaviours which at low frequencies may be modelled using the orientation distribution function (ODF) approach. However, the anisotropic behaviour of core losses at higher frequencies is rarely addressed. Therefore, this work aims to offer a method to model the anisotropy of these losses for a wide range of frequencies. This work proposes a modified approach that uses the ODF and the Kondorsky law to compute the core losses accurately in any direction for a wide range of frequencies so that the losses due to different magnetisation processes can be studied separately. The paper also highlights possible causes behind the anisotropic behaviour of the excess loss. The proposed approach is also compared with the original ODF description for modelling the loss behaviour along arbitrary directions. The computed loss-frequency behaviour at different induction levels agrees with measured ones along arbitrary directions. The proposed formulation can be used to estimate the losses of transformers and rotating machines as a function of magnetic field direction and frequency.

Keywords Anisotropy · Core loss · GO steel · Loss separation · Orientation distribution function

1 Introduction

Electromagnetic devices, like electric motors and transformers, are becoming the key components in emerging green technologies, including technologies that enable transportation electrification and renewable energy infrastructure. These devices mainly contain soft and hard magnetic materials; thus, their performance is significantly influenced by the quality of these materials. Hysteretic, dynamic, and anisotropic features in the magnetic behaviour of soft magnetic materials are well known [1–3]. Precise modelling of their magnetic characteristics and losses is a classical problem in the field of magnetism. Grain-oriented (GO) Si-Fe laminations are extensively used for magnetic circuits in transformers and some advanced rotating machines like axial flux machines [4–7]. GO laminations show anisotropic behaviour in their magnetic properties [8–11] because of the prominent crystallographic texture [12–14]. The performance of a magnetic material can be determined by the amount of dissipated heat energy in the magnetisation process, which is strongly dictated by the crystalline anisotropy [2]. Consequently, the materials can be textured to optimise magnetic

✉ Sai Ram Boggavarapu
sairam@iitdh.ac.in

1 Department of Electrical, Electronics, and Communication Engineering, Indian Institute of Technology Dharwad, Dharwad 580011, India

2 Division of Critical Materials, US Department of Energy, Ames National Laboratory, Ames, IA 50011, USA

3 Department of Electrical Engineering, Czestochowa University of Technology, Czestochowa, Poland

4 Department of Electrical Engineering, Indian Institute of Technology Bombay, Mumbai 400076, India

5 Laboratoire de Génie Electrique Et Electronique de Paris, Université Paris-Saclay, CentraleSupélec, CNRS, 91192 Gif-Sur-Yvette, France

6 Laboratoire de Génie Electrique Et Electronique de Paris, Sorbonne Université, CNRS, 75252 Paris, France

7 Universidade Federal Flumiennse, Av. Dos Trabalhadores, 420 - Vila Santa Cecilia, Volta Redonda, RJ 27255-125, Brazil

Published online: 08 January 2025

properties in particular directions, also known as easy directions, compared to the other directions. Fe-Si GO steel laminations have the rolling direction (RD) along one of the easy directions, and they have the best properties along RD. The shapes of hysteresis loops and losses at different angles due to the complex magnetisation process in GO laminations (grade 27M-OH) are given in Fig. 1.

Understanding of the complex magnetisation process in GO laminations is essential for designers facing efficiency improvement challenges of reducing machine loss without increasing cost. In modern electric machines, particularly power transformers and large rotating machines, the magnetic flux may not always be along the rolling direction (easy direction). Generally, the flux deviates from RD in corners and T-joint regions in transformers and at tooth-yoke joint regions in rotating machines [15], as depicted in Fig. 2. Thus, these regions are known to have significant loss contribution as the flux deviates from RD and encounter the poor magnetic properties of the core material. Moreover, accurate computations of core losses in electrical machines also require considering the anisotropy and frequency dependence [16–20]. Hence, a comprehensive formulation to predict the loss behaviour in arbitrary directions and excitation frequency is essential for selection of material and optimisation of electrical machines [21–23]. Also, the angular behaviour of core losses at higher frequencies needs further modifications in the existing loss models [24].

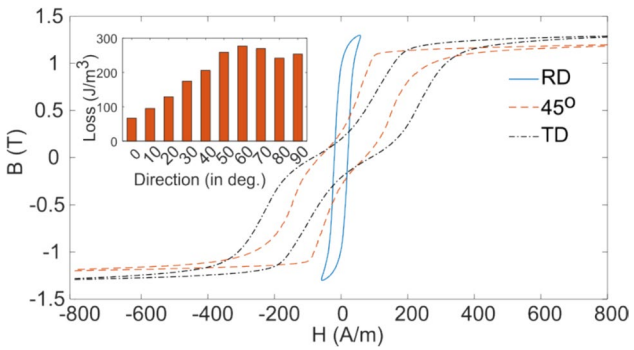

Fig. 1 Measured hysteresis loops and losses (inset) of iron-silicon steel (grade—27 M-OH/0.27 mm thick laminations) at different angles (RD, rolling direction; TD, transverse direction)

When these electrically conductive materials are subjected to time-varying excitations, eddy currents are induced, which in turn leads to energy conversion into heat [4, 25–27]. For uniform flux distribution, an analytical expression for these losses can be derived from Maxwell's equations [4, 28]. The measured values of losses generally exceed those calculated from the classical theory, and the difference is often attributed to material inhomogeneity (presence of domains) as the classical theory assumes homogeneous properties [25–28]. In [25], it is reported that the dynamic loss component depends on the ratio of the domain spacing to the sheet thickness. A subsequent refinement of the theory introduced by the Italian school of magnetism [26, 29] presents an excess loss component (P_{ex}) in addition to the hysteresis loss (P_h) and the classical eddy current loss. The loss components appearing at different spatial scales of the magnetisation process make the analysis a multi-scale problem [21, 30]. Moreover, the situation becomes even more complicated due to significant anisotropy of magnetic properties, including loss behaviour in GO steel laminations [8–11].

The anisotropic behaviour is well-studied for hard magnetic materials [7, 31–35]in which its optimisation enables the manufacturing of high-performance permanent magnets. On the contrary, the topic is rarely addressed for soft magnetic materials in the literature [37, 38]. Numerous attempts to model the anisotropic behaviour of electrical steels have been reported in the literature [24, 38–51]. The anisotropic behaviour of electrical steels is also modelled in terms of

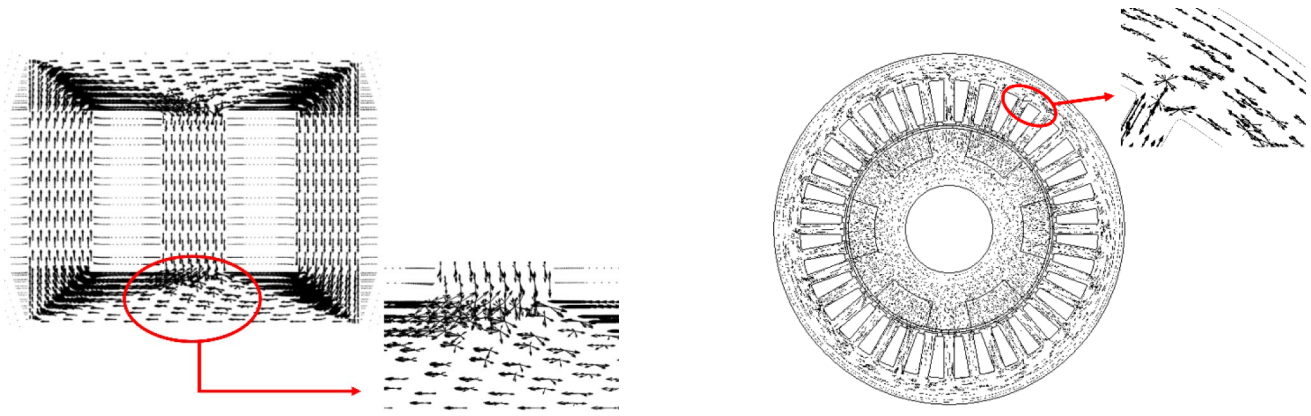

Fig. 2 Magnetic field distribution at **a** T-joints of a transformer [4] and **b** teeth-yoke joints of a motor [19]

cubic splines [38], loss components [39], and elliptical functions [40]. Another approach based on co-energy [41, 42] is also commonly used to model the anisotropy behaviour. The co-energy-based approach is easy to implement numerically with prior knowledge of the properties along the two principal (rolling and transverse) directions. The model has been applied to formulate the anisotropic behaviour at arbitrary angles for GO steels [42]. A modification in the Jiles-Atherton (JA) model to consider the effect of anisotropy on the quasi-static hysteresis loop has been proposed in [24]. This formulation can successfully approximate hysteresis loops in arbitrary directions, although it is limited to the quasi-static loss term due to hysteresis only. A method based on the relationship between crystallographic texture and magnetic properties, known as orientation distribution function (ODF), is reported in [12, 43, 44]. This formulation can predict physical properties of interest using the first three ODF coefficients [12]. This approach has been successfully applied to GO steel laminations for predicting their anisotropic magnetic behaviour [39, 45, 46]. The ODF model can also formulate the core losses' anisotropic behaviour when the predominant magnetisation process is the domain magnetisation rotation. However, it may yield erroneous results in modelling the anisotropic behaviour of the core losses, for instance, at high frequencies when the excess loss component is significant, as pointed out in [12]. Yet another work reported a hybrid approach; the co-energy approach is combined with the ODF method to predict the magnetic behaviour of GO materials [47]. In [48], a vectorisation technique is applied to the JA model to describe the anisotropic magnetic characteristics of non-oriented materials. An interesting approach which separates core losses into low and high induction loss components is reported for non-oriented (NO) materials [49–51]. The anisotropy in the high induction loss component is attributed to crystallographic texture, which in the low induction component is due to the variation in pinning sites with direction [36].

This paper aims to offer a comprehensive model for anisotropy in loss behaviour over a wide range of frequencies. The quasi-static hysteretic characteristics are explained in terms of domain magnetisation rotation and domain wall displacements, and the magnetisation rotation mechanism becomes predominant in directions other than the rolling direction (RD) [13, 36]. The anisotropic behaviour of the domain wall displacement mechanism is described by Kondorsky law [31, 33]. On the other hand, the anisotropy in the domain magnetisation rotation mechanism can be explained in terms of Bunge anisotropy [12]. The loss components that depend on microstructural features of the material, viz., the static hysteresis and excess loss components, exhibit significant anisotropy [11, 12]. The anisotropy of these two loss components is modelled using a generalised approach based on the ODF and the Kondorsky theory. Classical eddy current loss depends on the electric conductivity and thickness of the sample [52, 53]. The electrical conductivity can reasonably be considered as isotropic [4]. Hence, this component can be assumed constant for all directions. This work is devoted to studying the angular behaviour of different loss components and developing an adequate model to compute core losses accurately in any direction. Computed loss data are shown to be in close agreement with measurements. The proposed formulation is also compared with the original ODF approach for predicting the angular behaviour of the core losses.

2 Core Loss Modelling

2.1 Measurement of Magnetic Hysteresis Loops

Samples of a GO material (grade—27M-OH) cut at angles of 0°, 10°, 20°,…, 90° with respect to the rolling direction (RD) are used for measurements. The samples were cut mechanically with special care to avoid significant mechanical stress at the cutting edges. Two additional samples cut at angles 22.5° and 45° are also used to aid parameter identification. The thickness, length, and width of the samples are 0.27 mm, 200 mm, and 29.5 mm, respectively, and a standard single sheet tester (BROCKHAUS MPG 200D) was used for measurements. Although experiments were performed with sinusoidal waveforms of magnetic flux density (peak values range from 0.1 to 1.3 T) over the frequency range of 5–200 Hz, some deviations from the sine shape of B waveform were observed for 40°–70° angles. Therefore, it is logical to compute the loss by integrating B-H loop data. Measurements at higher induction levels ($B > 1.3$ T) need very high H fields (or current (I) values), particularly for 40°–60° samples due to the highly anisotropic nature of the material. Therefore, the measurements are limited to peak induction values (B) up to 1.3 T and frequencies up to 200 Hz.

2.2 Loss Separation Theory

As discussed earlier, losses in a soft magnetic material can be separated into static hysteresis loss, classical eddy current loss, and excess loss [53]:

$$W_{\text{tot}} = W_{\text{h}} + W_{\text{cl}} + W_{\text{ex}} \tag{1}$$

where W_{tot} represents the total core loss, W_{h} is the static hysteresis loss, W_{cl} is the classical eddy current loss, and W_{ex} is the excess or anomalous loss.

The static hysteresis loss can be explained by the energy dissipated as the domain walls are unpinned from defects [30]. This term can be calculated using the area of the hysteresis loop when frequency approaches zero. The component

depends on various microstructural parameters (domain configuration, pinning site density, etc.) of the material [24, 54]. The classical eddy current loss is given as [53]:

$$W_{\mathrm{cl}} = k_{\mathrm{e}} \int \left(\frac{dB}{dt}\right)^2 dt = k_{\mathrm{e}} \int \left(\frac{dB}{dt}\right) dB \tag{2}$$

and $k_{\mathrm{e}} = \frac{d^2}{12\rho}(\mathrm{m}/\Omega)$

Here, d is the thickness and ρ is the electrical resistivity of the core material.

The excess loss is the spatial eddy current loss associated with local changes in magnetisation due to domain wall motion [25]. It can be modelled as [53]:

$$W_{\mathrm{ex}} = k_{\mathrm{ex}} \int \left(\frac{dB}{dt}\right)^{3/2} dt \simeq k_{\mathrm{ex}} \int \left|\frac{dB}{dt}\right|^{-1/2} \left(\frac{dB}{dt}\right) dB \tag{3}$$

Here, k_{ex} $((A/\Omega)^{-1/2})$ is the excess loss coefficient. The expression described here is a simplified version of Bertotti's formula for excess loss in GO materials, which is valid for the considered frequency range [26]. It depends on microstructural parameters (the number of domain walls and the spacing between two adjacent domain walls) in the material [29, 30].

2.3 Computation of Loss Components

The total core losses in magnetic materials can be formulated in terms of the summation of the three loss components:

$$\int H \cdot dB = W_{\mathrm{h}} + k_{\mathrm{e}} \int \left(\frac{dB}{dt}\right) dB + k_{\mathrm{ex}} \int \left|\frac{dB}{dt}\right|^{\frac{-1}{2}} \left(\frac{dB}{dt}\right) dB \tag{4}$$

The three loss components are represented in integral form, which enables the approach to consider arbitrary waveforms of induction B. The classical eddy current loss (W_{cl}) is computed using (2)—the parameter k_{e} depends on the resistivity ($\rho = 4.6 \times 10^{-7}$ Ω-m) and the thickness ($d = 0.27$ mm). The other two loss components can be calculated by determining their coefficients (k_{ex} and W_{h}). By deducting the eddy current loss on both sides of (4), the loss equation can be formulated in a matrix form [55]:

$$[K][C] = [W] \tag{5}$$

Here,

$$K(i,:) = [1 \int \left|\frac{dB_i}{dt}\right|^{-\frac{1}{2}} \frac{dB_i}{dt} dB_i], i = 1 \text{ to } n, \tag{6}$$

and

$$W(i) = \int H_i dB_i - W_{\mathrm{cl}}(i) \tag{7}$$

i.e., a row of the matrices $[K]$ and $[W]$ corresponds to the loss at different frequencies (here, $n = 2$ represent two frequencies: 5 Hz and 200 Hz and they have been used in this analysis for parameter identification). The two unknowns $C(i) = [W_{\mathrm{h}}\ k_{\mathrm{ex}}]$ are calculated by solving a set of linear Eqs. (5) for a particular induction level. To demonstrate the model's prediction ability, the losses are computed at other frequencies not used in the parameter identification. The computed loss components for frequencies (5–200 Hz) at 1.1 T along different directions are shown in Fig. 3.

3 Modelling of Anisotropy in the Core Losses

The main origin of the anisotropic behaviour of GO laminations is crystalline anisotropy and crystallographic texture effects, as shown in Fig. 4. In a cubic crystal, the positive anisotropic constant (K_1) leads to six directions of minimum energy. They are in the direction of the magnetisation vectors along the three orthogonal easy axes (both positive and negative directions). For GO laminations, the [001] easy axis of crystallites is significantly aligned along RD, and their lamination surface is almost parallel to their (110) plane. This orientation is known as the Goss texture [29].

For these materials, magnetocrystalline anisotropy plays an important role in the phase equilibrium, and their magnetic characteristic along different directions can be derived from different forms of the phase equilibrium [8]. The magnetisation process involves rotating the magnetisation vector and domain wall motion [5, 13]. The former can be described by the Stoner-Wohlfarth law and the latter by the Kondorsky law [31]. The hysteresis loss component depends on the domain configuration and crystallographic orientations [12, 45] and is modelled using the ODF approach. The approach can be used successfully to describe the anisotropic behaviour of the core losses strongly linked to irreversible

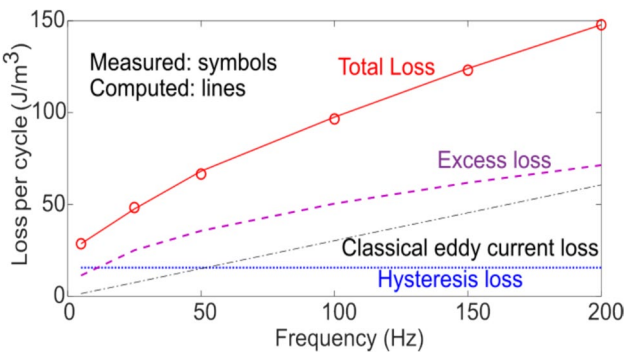

Fig. 3 Comparison of measured and calculated losses with frequencies for maximum flux density of 1.1 T (plain dots are shown in the figure to indicate the data used for parameter identification)

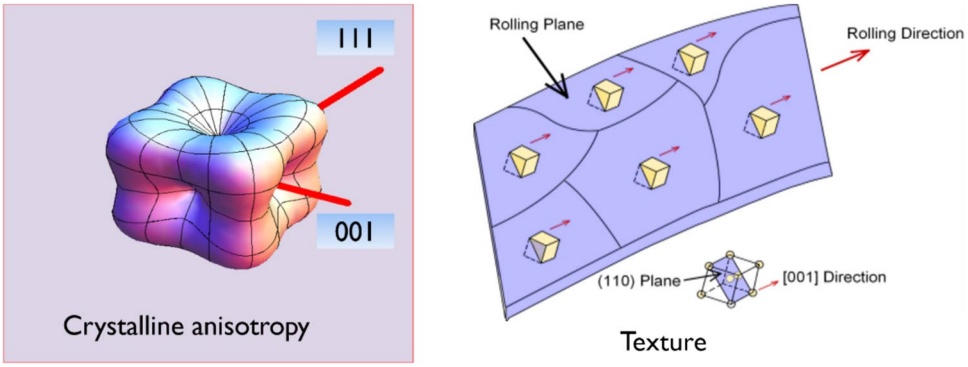

Fig. 4 Cubic crystalline and texture arrangement in a Fe-Si sheet (001) plane

domain magnetisation rotation. The approach can describe the quasi-static core losses with reasonable accuracy. However, it may lead to erroneous results at higher frequencies as it does not consider the loss related with the irreversible domain wall motion [31]. The anisotropy of irreversible domain wall motion can be modelled using Kondorsky law.

3.1 Bunge Anisotropy (ODF Approach)

For cubic crystalline materials, the magnetocrystalline anisotropy energy (E_{an}) is [12]:

$$E_{an} = K_0 + K_1\left(\alpha_1^2\alpha_2^2 + \alpha_2^2\alpha_3^2 + \alpha_3^2\alpha_1^2\right) + K_2\alpha_1^2\alpha_2^2\alpha_3^2 \tag{8}$$

Here, K_0, K_1, and K_2 are the magnetocrystalline anisotropy constants and depend on the material and α_1, α_2, and α_3 are the directional cosines of the magnetisation vector measured from the three crystal axes.

The ODF can be derived from magnetocrystalline anisotropy due to a combination of cubic symmetry and orthorhombic sheet symmetry [13]. Hence, for the GO laminations, the ODF function can be represented as [44]:

$$E(\theta) = E_0 + E_1 cos(2\theta) + E_2 cos(4\theta) \tag{9}$$

where E represents the average of any of the physical properties (permeability, iron losses, magnetic induction) of electrical steels, and E_0, E_1, and E_2 are anisotropy constants. It is important to note here that Eq. (9) describes in-plane anisotropy for GO lamination sheets [24]. However, the ODF considers only the magnetisation rotation mechanism and hence the crystallographic features [13, 43]. In the above equation, E_0 represents an averaged magnetic property. The parameters E_1 and E_2 are close to zero if properties of the material under consideration are isotropic. Deviation of the values of these parameters from zero indicates an increase in anisotropy [46]. The angular dependence of the three factors (Eq. 9) is shown in Fig. 5.

In GO materials, the core loss shows a strong dependence on crystallographic features [42, 53]. The loss W correlates with the projection P < 100 > of the < 100 > crystallographic

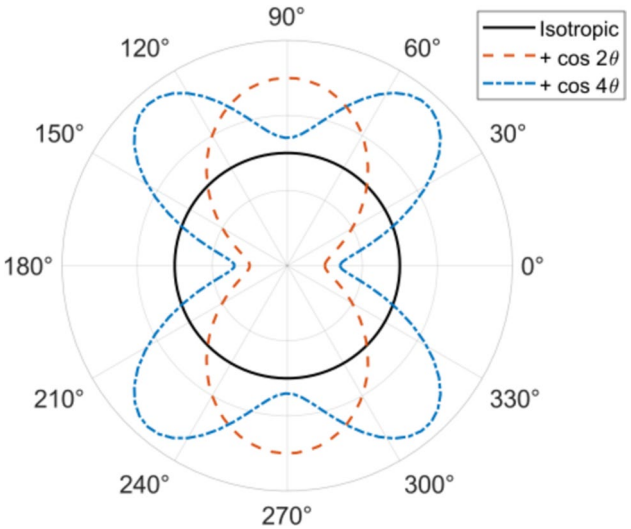

Fig. 5 Angular dependence of Eq. (9) with each of the anisotropy components considered

directions (easy axes) along the macroscopic directions from RD to TD, as defined in [56]. The loss behaviour is predominantly related to the crystallographic texture, as shown in Fig. 6. These projections have been calculated from the crystallographic texture data typical of a GO material [22].

3.2 Kondorsky Law

The Kondorsky law relates the domain wall (DW) pinning field (or coercivity) to the variation of the DW surface energy density with respect to the domain wall displacement [33]. The anisotropic behaviour of domain wall displacements follows the Kondorsky rule [31]. The angular variation (in plane 0 to 90) of the losses associated with the domain wall motion can be represented as [31]:

$$W_K(\theta) = \frac{W_K}{cos(\theta)} \tag{10}$$

Equation 10 can be rewritten as:

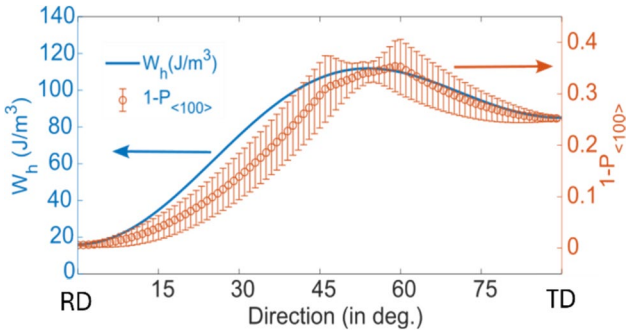

Fig. 6 Modelled static hysteresis loss and correlation with projections P < 100 > of the < 100 > crystallographic directions (easy axes), as defined in [56]

$$W_K(\theta) = \frac{W_K}{cos(b * \theta)} \tag{11}$$

The coefficient b is used to avoid the asymptotically increasing behaviour of the above function at $\theta = 90°$. The value of b is taken as 0.95 in this analysis.

3.3 Anisotropy in the Core Loss Components

A generalised expression of the total core loss with the anisotropy consideration can be written as:

$$W(f, \theta) = W_h(\theta) + W_{cl}(f) + W_{ex}(f, \theta) \tag{12}$$

The static hysteresis loss W_h (θ) is measured in a quasi-static condition, which varies with direction. The classical eddy current loss W_{cl} (θ) depends on frequency, but the component remains the same in all directions. The excess loss component W_{ex} (θ) depends on frequency and direction. The total anisotropy in these loss components can be represented as the sum of two contributions associated with the Bunge (ODF) anisotropy (domain magnetisation rotation) and the Kondorsky law (domain wall motion) as:

$$W(\theta) = W_0 + W_1 cos(2\theta) + W_2 cos(4\theta) + W_K \left(\frac{1}{cos(b*\theta)} \right) \tag{13}$$

where W can be W_h or W_{ex}; the ODF coefficients are W_0, W_1, and W_2. The last term represents the angular dependency of losses associated with domain wall displacement.

The total loss is obtained by computing each of the three loss components in any direction using (13). The loss components along four distinct directions—0°, 22.5°, 45°, and 90°—are used to calculate the model parameters. Thus, the parameters can be determined by using a set of four linear equations obtained from the loss and coefficient values:

Table 1 Anisotropic loss model coefficients

Static loss coefficients	Values (J/m^3)	Excess loss coefficients	Values (A/Ω)$^{-1/2}$
W_{h0}	61.13	k_{ex0}	1.53
W_{h1}	−27.23	k_{ex1}	−0.78
W_{h2}	−19.44	k_{ex2}	−0.25
W_{hK}	1.23	c_{heck}	0.0048

$$\begin{bmatrix} F(0) \\ F\left(\frac{\pi}{8}\right) \\ F\left(\frac{\pi}{4}\right) \\ F\left(\frac{\pi}{2}\right) \end{bmatrix} = \begin{bmatrix} 1 & 1 & 1 & 1 \\ 1 & 0.7071 & 0 & 1.0739 \\ 1 & 0 & -1 & 1.3618 \\ 1 & -1 & 1 & 12.7455 \end{bmatrix} \begin{bmatrix} F_0 \\ F_1 \\ F_2 \\ F_3 \end{bmatrix} \tag{14}$$

Here, F can be W_h or K_{ex}. The values in the fourth column of the matrix in (14) are greater than unity and as $\theta \rightarrow 90^{\circ}$ the values in this column will be much greater than unity because of the 1/cos (b*θ) term; thus, they significantly differ from values in other columns. The obtained model parameters can be applied to calculate losses for different frequencies and directions.

4 Results and Discussions

The core losses are computed using the identified loss coefficients in Sect. 2.3. The measured loss values at $B_m = 1.1$ T and the frequencies (5 Hz and 200 Hz) for four directions have been used in this analysis for parameter identification. The obtained parameters are presented in Table 1.

Using the parameters, the core losses are computed for 50 Hz and 100 Hz (which are not used in the parameter identification) along different directions, as shown in Fig. 7. Anisotropic behaviours of the different loss components are shown in Fig. 7 for $B_m = 1.1$ T, $f = 50$ Hz, and $f = 100$ Hz.

The difference in angular variations of the static hysteresis and excess loss components (as shown in the above figure) can be explained by different contributions from the two distinct mechanisms of domain wall motion and domain magnetisation rotation.

4.1 Comparison with the ODF Approach

The core loss is computed using the proposed approach and compared with the loss obtained using the original ODF approach [42], as shown in Fig. 8. Table 2 lists the parameters of the initial ODF method, which were determined using the core loss at 1.1 T and 5 Hz along three directions (0°, 45°, and 90°).

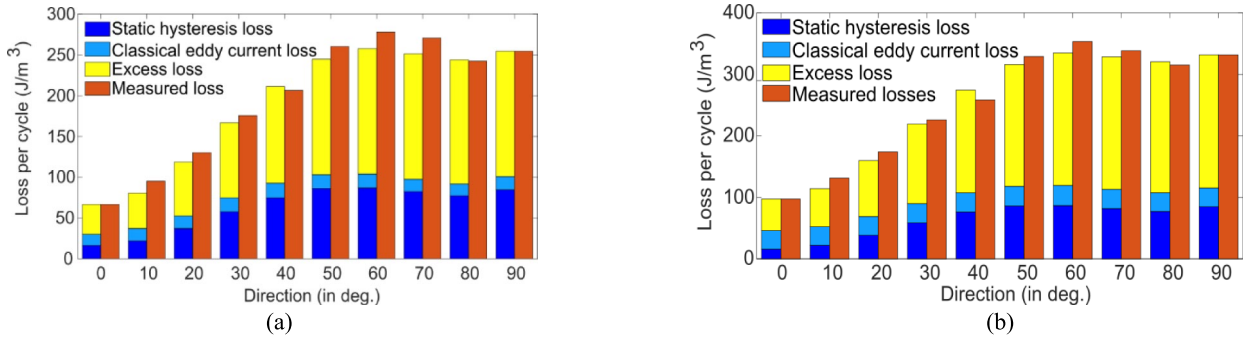

Fig. 7 Anisotropic behaviour of loss components at $B_m = 1.1$ T for **a** 50 Hz and **b** 100 Hz

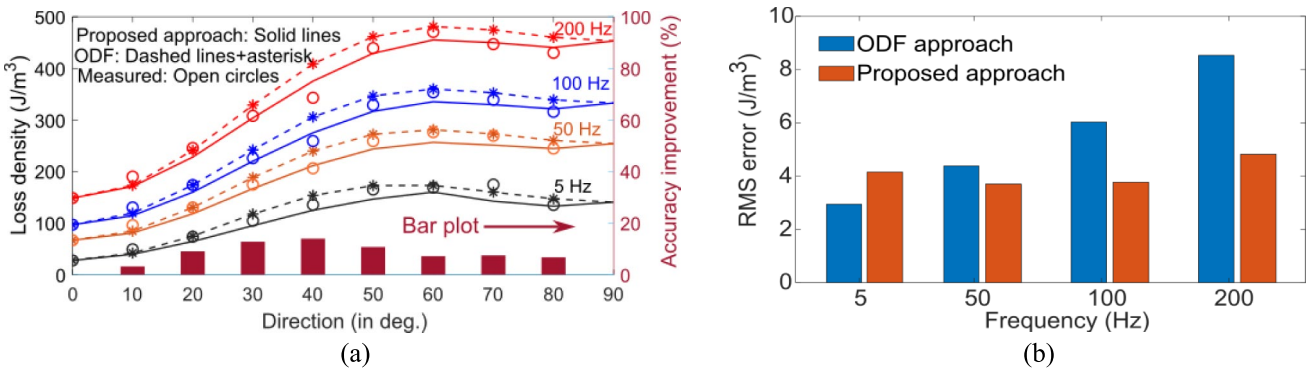

Fig. 8 **a** Comparison of calculated and measured total loss at 1.1 T. The bar graphs (2nd *Y*-axis) show the difference in the average errors, which indicates the accuracy improvements of the proposed approach over the ODF. **b** Comparison of RMS errors (for all directions) at different frequencies

Table 2 ODF coefficients

ODF coefficients	Values (J/m^3)
E_0	110.34
E_1	−56.47
E_2	−25.79

Using the averaged errors of different frequencies along arbitrary directions, Fig. 8a displays a bar plot illustrating the accuracy improvement with the suggested formulation over the ODF technique. It quantifies the improvement in accuracy of the predicted losses using the proposed approach and shows its effectiveness over the ODF approach in any direction. It is also important to note here that the proposed approach requires losses in four directions (an additional direction compared to the ODF method) at two frequencies (here, 5 and 100 Hz) for parameter identification.

The following formula is used to determine the root mean square errors (RMSEs) for all directions at various frequencies.

$$RMSE = \sqrt{\sum_{i=1}^{N} \frac{\left(W(f,\theta_i) - W_{tot}(f,\theta_i)\right)^2}{N}} \tag{15}$$

where $W(f, \theta_i)$ is calculated using (12), $W_{tot}(f, \theta_i)$ is the measured value at frequency f, and $\theta_i = [0°, 10°, 20°, \ldots, 90°]$. The errors in computed losses using the two approaches are quantified in Fig. 8b. It shows the predicted result that compares relatively well with the experimental results with respect to the angular behaviour of the losses. Thus, the proposed generalised approach predicts the loss more accurately than the ODF approach at higher frequencies, as clearly evident from Fig. 8b. This is logical since the contribution of domain wall motion will increase at higher frequencies, which is accounted for by the Kondorsky function in the proposed model. Therefore, a modification of the original ODF function, as herein presented, is recommended to predict anisotropy in the core losses over a wide range of frequencies. In other words, to accurately predict the angular behaviour of the core losses, it is essential to consider the anisotropy of both domain magnetisation rotation and domain wall motion.

Table 3 Static loss coefficients at different induction levels

Static loss coefficients	$B_m = 0.5$ T	$B_m = 0.7$ T	$B_m = 1.3$ T
W_{h0} (J/m^3)	19.17	34.46	115.4
W_{h1} (J/m^3)	−8.83	−23.66	−60.23
W_{h2} (J/m^3)	−8.05	−4.11	−31.96
W_{hK} (J/m^3)	0.0048	0.0063	0.57

Table 4 Excess loss coefficients at different induction levels

Excess loss coefficients	$B_m = 0.5$ T	$B_m = 0.7$ T	$B_m = 1.3$ T
k_{ex0} (A/Ω)$^{-1/2}$	1.21	1.22	1.55
k_{ex1} (A/Ω)$^{-1/2}$	−0.72	−0.73	−0.79
k_{ex2} (A/Ω)$^{-1/2}$	−0.18	−0.22	−0.25
k_{exK} (A/Ω)$^{-1/2}$	0.0032	0.0036	0.0048

4.2 Loss Model at Different Induction Values

The approach is also applied to the losses at different induction levels (0.5, 0.7, and 1.3 T). The loss model parameters for each induction level can be obtained by applying the identification approach discussed earlier in Sect. 3. The obtained hysteresis loss and excess loss coefficients are given in Tables 3 and 4 for different induction levels. Anisotropy constants in the loss behaviours at 0.5 T, 0.7 T, and 1.3 T are shown in Fig. 9a–c. In addition, the figures also include a bar graph that quantifies the average error magnitude for all frequencies along each direction, demonstrating the effectiveness of the suggested strategy at different frequencies and along any direction. Furthermore, the magnitudes of the RMSEs (of all directions) for the losses calculated at different frequencies/flux densities are given in Fig. 9d.

From Fig. 9d, it can be observed that the RMS error (in J/m^3) is increasing with the frequency. This is because the net loss also increases with frequency. So, the calculated RMS error is less than the loss value at the corresponding frequency. In the current work, in the measurement setup, the magnetic flux density waveform is programmed to be a sinusoidal waveform; because of the limitations of the measurement setup, the waveform deviated. To validate the accuracy of the proposed formulation, the measured magnetic flux density waveform is used to calculate the losses. In the case of non-sinusoidal flux waveforms, which practically occur in transformers and rotating machines, the losses can be calculated using time-dependent expressions (Eqs. 2–4), or frequency components of flux density can be evaluated using Fourier analysis and loss at each component in the frequency domain can be calculated. The use of Fourier analysis to estimate the losses for non-sinusoidal flux density waveforms is identified as future work.

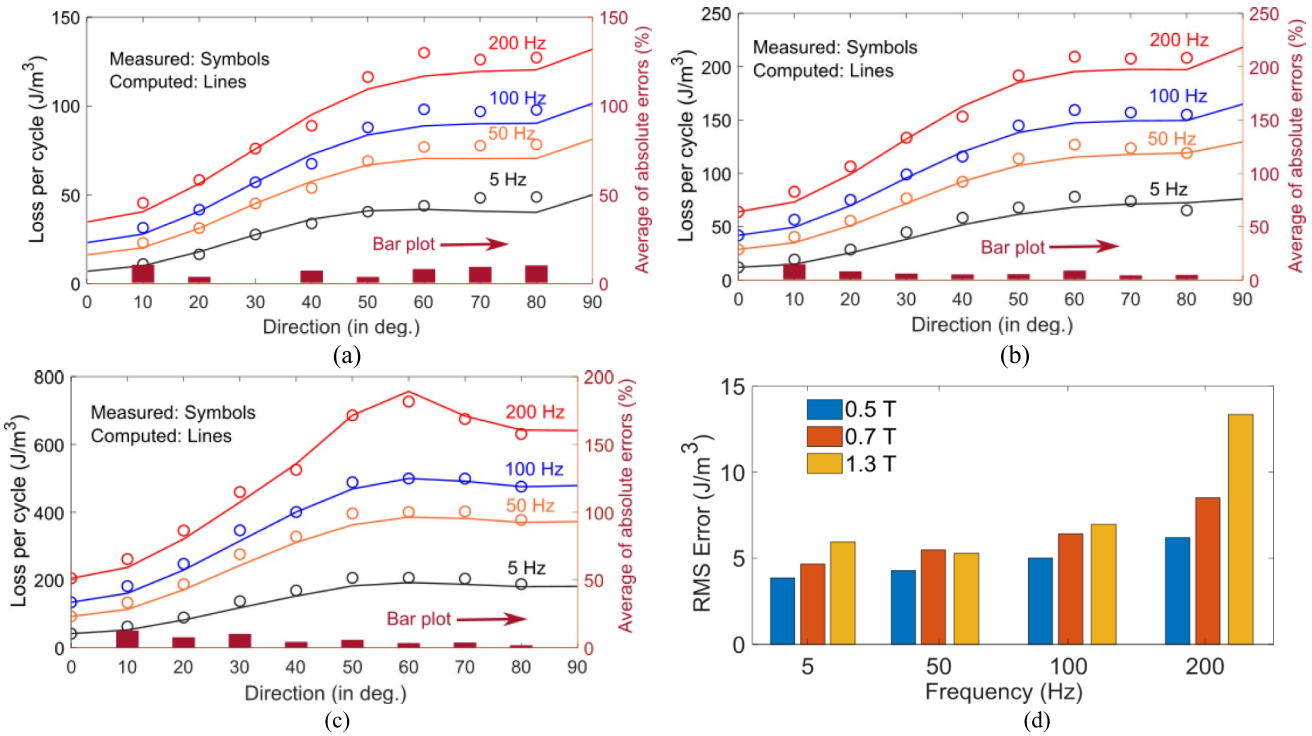

Fig. 9 Comparison of calculated and measured losses with direction (the bar graphs (2nd *Y*-axis) show the average of absolute errors) at different frequencies for **a** $B_{max} = 0.5$ T, **b** $B_{max} = 0.7$ T, **c** $B_{max} = 1.3$ T, and **d** RMS error of computed and measured losses for the flux densities shown in **a**–**c**

5 Conclusion

This work proposes a comprehensive formulation to model the anisotropic behaviour of the losses in GO laminations using the loss separation approach. The anisotropic behaviour of loss components, mainly static hysteresis loss and excess loss, is formulated in terms of the two magnetisation mechanisms: domain magnetisation rotation and domain wall displacement. The classical eddy current loss is not dependent on the direction of magnetisation. The anisotropic behaviour of the core loss is modelled using the magnetisation rotation—domain wall displacement (Bunge ODF-Kondorsky function) model. Each level of induction and each component of loss (static hysteresis loss and excess loss) requires the identification of four parameters (three ODF coefficients and one Kondorsky function parameter) using the measured magnetic losses in four directions (0°, 22.5°, 45°, and 90°) at two frequencies only.

The proposed approach is also compared with the original ODF approach in the paper. The suggested approach can predict the angular loss behaviour for a wider frequency range of up to 200 Hz. The approach is applied for induction levels up to 1.3 T and it gives satisfactory results. This method would be helpful in modelling the total core loss when magnetic fields are not aligned with the two principal directions, such as in the core joints of transformers.

Acknowledgements The authors would like to thank Crompton Greaves Ltd., Mumbai, India, for providing experimental facilities. This work was partly performed at Ames National Laboratory, operated for the US Department of Energy by Iowa State University of Science and Technology under Contract No. DE-AC02-07CH11358.

Author Contributions The research work is conceptualized by Dr. A. P. S. Baghel, Dr. K. Chwastek, Prof. L. Daniel, and Prof. M. F. de Campos. Dr. B. Sai Ram, Dr. A. P. S. Baghel, and Dr. I. C. Nlebedim did the simulations, prepared figures, and wrote the main text. Dr. A. P. S. Baghel and Prof. S. V. Kulkarni have done the experimental measurements. All the authors reviewed the manuscript.

Data Availability No datasets were generated or analysed during the current study.

Declarations

Competing Interests The authors declare no competing interests.

References

1. Fiorillo, F., Bertotti, G., Appino, C., Pasquale, M.: Soft magnetic materials in Wiley Encyclopedia of Electrical and Electronics Engineering, 1–42, 2016
2. Ducharne, B., Zurek, S., Daniel, L., Sebald, G.: An anisotropic vector hysteresis model of ferromagnetic behavior under alternating and rotational magnetic field, J. Magn. Magn. Mater. **549**, 2022, Art. No. 169045
3. Chen, J., Shang, H., Xia, D., Wang, S., Peng, T., Zang, C.: A modified vector Jiles-Atherton hysteresis model for the design of hysteresis devices. IEEE Trans. Energy Convers. **38**(3), 1827–1835 (2023)
4. Kulkarni, S.V., and Khaparde, S.A.: Transformer engineering: design, technology, and diagnostics, Second Edition, Boca Raton: CRC Press (Taylor & Francis Group), 2012.
5. Sai Ram, B., Paul, A.K., Kulkarni, S.V.: Soft magnetic materials and their applications in transformers J. Magn. Magn. Mater **537**, 2021, Art. No. 168210.
6. Ma, J., et al.: Optimal design of an axial-flux switched reluctance motor with grain-oriented electrical steel. IEEE Trans. Ind. Appl. **53**(6), 5327–5337 (2017)
7. Fan, L.F., Dong, R.F., Qiu, S.T., Xiang, L., Tang, G.B.: Effect of Sn on high permeability grain-oriented silicon steel. J. Supercond. Novel Magn. **27**, 1959–1965 (2014)
8. Fiorillo, F., Dupre, L.R., Appino, C., Rietto, A.M.: Comprehensive model of magnetization curve, hysteresis loops, and losses in any direction in grain-oriented Fe–Si. IEEE Trans. Magn. **38**, 1467–1476 (2002)
9. Dupré, L.R., Fiorillo, F., Melkebeek, J., Rietto, A.M., Appino, C.: Loss versus cutting angle in grain-oriented Fe–Si laminations. J. Magn. Magn. Mater. **215–216**, 112–114 (2000)
10. Paltanea, V., Paltanea, G.: Study of the magnetic anisotropy of the grain oriented (GO) and non-oriented (NO) silicon iron materials. Mater. Sci. Forum **670**, 66–73 (2009)
11. Shin, S., Schaefer, R., DeCooman, B.C.: Anisotropic magnetic properties and domain structure in Fe 3%Si (110) steel sheet J. Appl. Phys. **109**, 1–3, 2011, Art no. 07A307.
12. de Campos M.F.: Anisotropy of steel sheets and consequence for Epstein test: I theory in Proc. XVIII IMEKO Congress, Rio de Janeiro, Brazil, 2006.
13. de Campos, M.F., Campos, M.A., Landgraf, F.J.G., Padovese, L.R.: Anisotropy study grain-oriented steels with magnetic Barkhausen noise J. Phys.-Conf. Series, vol. 303, pp. 1–6, 2011, Art no. 1012020.
14. de Campos, M.F.: Methods for texture improvement in electrical steels. Przegląd Elektrotechniczny **95**, 7–11 (2019)
15. Zurek, S.: Characterisation of soft magnetic materials under rotational magnetisation. CRC Press, London, U.K. (2017)
16. Zhang, Y., Wang, J., Sun, X., Bai, B., Xie, D.: Measurement and modeling of anisotropic magnetostriction characteristic of grain-oriented silicon steel sheet under DC bias IEEE Transact. Magnet **50** 1–4, 2014, Art no. 7008804
17. Guo, Y., Zhu, J.G., Zhong, J., Lu, H., Jin, J.X.: Measurement and modeling of rotational core losses of soft magnetic materials used in electrical machines: a review. IEEE Trans. Magn. **44**, 279–291 (2008)
18. Pfützner, H., Mulasalihovic, E., Yamaguchi, H., Sabic, D., Shilyashki, G., Hofbauer, F.: Rotational magnetization in transformer cores - a review. IEEE Trans. Magn. **47**, 4523–4532 (2011)
19. Leite, J.V., Ferreira da Luz, M.V., Sadowski, N., da Silva, P.A., Jr.,: Modelling dynamic losses under rotational magnetic flux. IEEE Trans. Magn. **48**, 895–898 (2012)
20. Zurek, S,: Qualitative analysis of Px and Py components of rotational power loss IEEE Transact. Magnet. **50**, 1–14, 2014, Art no. 6300914
21. de la Barrière, O., Ragusa, C., Appino, C., Fiorillo, F.: Prediction of energy losses in soft magnetic materials under arbitrary induction waveforms and dc bias. IEEE Trans. Industr. Electron. **64**, 2522–2529 (2017)
22. Hubert, O., Daniel, L.: Multiscale modeling of the magnetomechanical behavior of grain-oriented silicon steels. J. Magn. Magn. Mater. **320**, 1412–1422 (2008)
23. Demian, C., Cassoret, B., Brudny, J.F., Belgrand, Th.: AC magnetic circuits using nonsegmented shifted grain-oriented electrical steel sheets: impact on induction machine magnetic noise. IEEE Trans. Magn. **48**, 1409–1412 (2012)

24. Baghel, A.P.S., Sai Ram, B., Chwastek, K., Daniel, L., Kulkarni, S.V.: Hysteresis modelling of GO laminations for arbitrary in-plane directions taking into account the dynamics of orthogonal domain walls J. Magn. Magn. Mater. **418**, 14–20, 2016
25. Pry, R.H., Bean, C.P.: Calculation of the energy loss in magnetic sheet materials using a domain model. J. Appl. Phys. **29**, 532–533 (1958)
26. Bertotti, G.: Physical interpretation of eddy current losses in ferromagnetic materials. I. Theoretical considerations. J. Appl. Phys. **57**, 2110–2117 (1985)
27. Wang, W., Nysveen, A., Magnusson, N.: Eddy current loss in grain-oriented steel laminations due to normal leakage flux IEEE Transact. Magn. **57** 6, 1–4, 2021, Art no. 6301604
28. Zirka, S.E., Moroz, Y.I., Steentjes, S., Hameyer, K., Chwastek, K., Zurek, S., Harrison, R.G.: Dynamic magnetization models for soft ferromagnetic materials with coarse and fine domain structures. J. Magn. Magn. Mater. **394**, 229–236 (2015)
29. Bertotti, G.: *Hysteresis in magnetism*, San Diego. Academic, CA (1998)
30. Jiles, D.C.: Introduction to magnetism and magnetic materials. Chapman & Hall/CRC, Boca Raton (1998)
31. Deng H.Y., and Li Huang, H. Domain wall structure and the modified Kondorsky function Chin J. Phys. **39**, 479–497, 2001
32. Cimpoesu, D., Stoleriu, L., Stancu, A.: Generalized Stoner-Wohlfarth model accurately describing the switching processes in pseudo-single ferromagnetic particles J. Appl. Physic. **114**, 1–6, 2013, Art no. 223901
33. Givord, D., Tenaud, P., Viadieu, T.: Angular dependence of coercivity in sintered magnets. J. Magn. Magn. Mater. **72**, 247–252 (1988)
34. de Campos, M.F.: Effect of grain size, lattice defects and crystalline orientation on the coercivity of sintered magnets. Mater. Sci. Forum **530–531**, 146–151 (2006)
35. Ibrayeva, A., and Eriksson, S.: Dynamic modeling of a generator with anisotropic nonlinear permanent magnets in finite element method software *IEEE Transact. Magn.* **59**(9), 1–8, 2023, Art no. 7401308.
36. de Campos, M.F.: A general coercivity model for soft magnetic materials. Mater. Sci. Forum **727–728**, 157–162 (2012)
37. da Cunha, M.A., Zwirmann, N.C.S.B., Volgien, V.W., Germano, R.S., Landgraf, F.J.G., Yanomine, T., Takanohashi, R., de Lima N.B.: The angular dependence of magnetic properties of electrical steels 21st Annual Conf. Prop. Appl. Magn. Mater. Illin Instit. Technol. EUA, sem página, 2002
38. Martin, F., Singh, D., Rasilo, P., Belahcen, A., Arkkio, A.: Model of magnetic anisotropy of non-oriented steel sheets for finite-element method IEEE Transact. Magnet. **52**(3), 1–4, March 2016, Art no. 7002704.
39. Pluta, W.: Anisotropy of specific total loss components in Goss textured electrical steel J Magn. Magn. Mater. **499**, 1–5, 2020, Art. No. 166270.
40. Biró, O., Außerhofer, S.T., Preis, K., Chen, Y., A modified elliptic model of anisotropy in nonlinear magnetic materials COMPEL – Int. J. Comput Math. Electric. Elect. Eng. **29**, 1482–1492, 2010
41. Péra, TH., Ossart, FL., Waeckerlé. TH., Numerical representation for anisotropic materials based on coenergy modeling J. Appl. Phys. **73**, 6784–6786, 1993
42. Chwastek, K., Najgebauer, M., Szczygłowski, J., Wilczyński, W.: Modelling the influence of anisotropy on magnetic properties in grain-oriented steels. Przeglad Elektrotechniczny (Electrical Review) **3**, 126–128 (2011)
43. Birsan, M., Szpunar, J.A.: Anisotropy of power losses in textured soft magnetic materials. J. Appl. Phys. **80**, 6915–6919 (1996)
44. Szpunar, J.A.: Anisotropy of magnetic properties in textured materials. Textures and Microstructures **11**, 93–105 (1989)
45. Chwastek, K., Baghel, A.P.S., de Campos, M.F., Kulkarni, S.V., Szczygłowski, J.: A description for the anisotropy of magnetic properties of grain-oriented steels IEEE Transact. Magn. **52**, 1–5, 2015, Art no. 6000905
46. Pluta, W.A.: Angular properties of specific total loss components under axial magnetization in grain-oriented electrical steel. IEEE Trans. Magn. **52**(4), 1–12 (2016)
47. Najgebauer, M.: Scaling-based prediction of magnetic anisotropy in grain-oriented steels. Arch. Electr. Eng. **66**, 432–432 (2017)
48. Martin, F., Chen, R., Taurines, J., Belahcen, A., Anisotropic hysteresis representation of steel sheets based on a vectorization technique applied to Jiles-Atherton model IEEE Transact. Magn. Early Access
49. Landgraf, F.J.G., de Campos, M.F., Leicht, J.: Hysteresis loss subdivision. J. Magn. Magn. Mater. **320**, 2494–2498 (2008)
50. Landgraf, F.J.G., Yonamine, T., Emura, M., Cunha, M.A.: Modelling the angular dependence of magnetic properties of fully processed non-oriented electrical steel. J. Magn. Magn. Mater. **254–255**, 328–330 (2003)
51. da Silva, L.G., Bernard, L., Martin, F., Belahcen A., Daniel, L.: Multiaxial validation of a magneto-elastic vector-play model IEEE Transact. Magn. **59**(11), 1–10, Nov. 2023, Art no. 7301010
52. Jiles, D.C.: Modelling the effects of eddy current losses on frequency dependent hysteresis in electrically conducting media. IEEE Trans. Magn. **30**, 4326–4328 (1994)
53. Baghel, A.P.S., and Kulkarni, S.V.: Dynamic loss inclusion in the Jiles–Atherton (JA) hysteresis model using the original JA approach and the field separation approach IEEE Transact Magn. **50**(2), 369–372, 2014, Art no. 7009004
54. Baghel A.P.S., and Kulkarni, S.V.: Hysteresis modeling of the grain-oriented laminations with inclusion of crystalline and textured structure in a modified Jiles-Atherton model J. Appl. Phys. **133**, 1–3, 2013, Art. No. 043908
55. Hamimid, M., Mimoune, S.M., Feliachi, M.: Hybrid magnetic field formulation based on the losses separation method for modified dynamic inverse Jiles-Atherton model. Physica B **406**, 2755–2757 (2011)
56. Hubert, O., Daniel, L., Billardon, R.: Experimental analysis of the magnetoelastic anisotropy of a non-oriented silicon iron alloy. J. Magn. Magn. Mater. **254**, 352–354 (2003)